JJEE
Volume 11 | Number 4 | Pages 619-637

Jordan Journal of Electrical Engineering

ISSN (print): 2409-9600, ISSN (online): 2409-9619

Homepage: jjee.ttu.edu.jo

# Fault Tolerant Control for Modular Drive of a Double Stator Windings, Twelve-Phase Permanent Magnet Synchronous Motor

**Davood Maleki[1*], Abolfazl Halvaei Niasar[2]**

[1, 2] University of Kashan, Ravand Road, Kashan, P.O.BOX: 8731753153, Iran
Email: halvaei@kashanu.ac.ir

*Received: Apr 04, 2025* *Revised: Sep 02, 2025* *Accepted: Sep 02, 2025* *Available online: Jan 20, 2026*

***Abstract*—** This paper presents a fault-tolerant control strategy for a twelve-phase open-ended Permanent Magnet Synchronous Motor (PMSM) with double stator windings, designed for submarine propulsion systems. Each stator phase comprises two aligned windings positioned symmetrically opposite each other relative to the stator center. To enhance system reliability, modular architecture is adopted for both the motor and its drive system. Each stator winding is independently powered by a dedicated single-phase H-bridge inverter, with individual microcontrollers providing decentralized control. Due to the modular design, each phase operates in its own stationary reference frame. To mitigate torque ripples caused by higher-order harmonics in the back-EMF voltage, a harmonic current injection (HCI) strategy is introduced in the stationery reference frame alongside quasi-proportional resonant (QPR) current controllers. In the event of a phase failure, the proposed fault-tolerant control (FTC) method compensates by dynamically adjusting the amplitude and phase of the remaining healthy phases, thereby minimizing second-order torque ripple. The effectiveness of the proposed approach is verified through comprehensive Simulink simulations under various fault conditions, supplemented by experimental results.

***Keywords*—** Fault-tolerant control (FTC); Reliability; Drive; Twelve-phase PMSM; H-bridge inverter; Proportional-resonant controller.

## 1. INTRODUCTION

In some special applications such as military industries and electric drives used in submarines, high reliability of the drive system is an essential design requirement. To achieve this, in addition to using high-quality hardware and equipment, various measures are taken in both hardware and software. For example, in hardware, redundancy in equipment such as increasing the number of motor phases, increasing the number of switches, and using independent single-phase H-bridge inverters for each phase, redundancy in control systems and microcontrollers, and redundancy in the number of sensors are among these measures. Additionally, the use of fault-tolerant control (FTC) methods ensures that the drive system can continue operating without significant disruption during faults [1].

In electric drive systems for marine vessels, especially submarines, PMSMs are particularly favored due to their high-power density, high torque, high efficiency, and sufficient reliability. Although three-phase PMSMs have adequate reliability, a fault in one of the three-leg inverter switches or one of the windings can cause a problem in the drive system. To further increase the reliability of the drive system, especially in high-power applications, multiphase PMSMs have attracted the attention of researchers and industry professionals in

* Corresponding author
DOI: https://doi.org/10.5455/jjee.204-1743771454

these sensitive applications. Increasing the number of phases reduces phase current and also mitigates the issues of motor losses and cooling [2]. Consequently, multi-phase PMSMs with multiple three-phase windings (6, 9, and 12 phases) have been used in medium to high-power applications. In high-power applications, the use of a modular design in both the motor and the power and control systems maximizes the reliability of the drive.

Multiphase motors are divided into two main categories: symmetric and asymmetric. In the symmetric type, the angle between the axes of all windings is equal, while in the asymmetric type it is not. Fig. 1 shows two commonly used types of twelve-phases PMSM drives [3]. In Fig.1(a) shows the design of an asymmetric twelve-phase PMSM with four sets of three-phase windings. This includes four sets of three-phase star-connected windings, with an angle of $30^{o}$ between two same windings in two adjacent sets. These four three-phase sets have only one star point and are powered by four independent three-phase inverters [4]. Fig. 1(b) illustrates a symmetric twelve-phase motor, where each phase is powered by an independent single-phase H-bridge inverter [5]. This design provides the highest level of reliability because if a fault occurs in one winding or one H-bridge inverter, the remaining motor phases continue to produce torque. This structure is practically designed and implemented in a modular form. In this paper, a design similar to the modular design in Fig. 1(b) is used to ensure maximum reliability. In the proposed design, each motor winding has two parts, located on opposite sides of the stator circumference, and is referred to as the double winding twelve-phase PMSM.

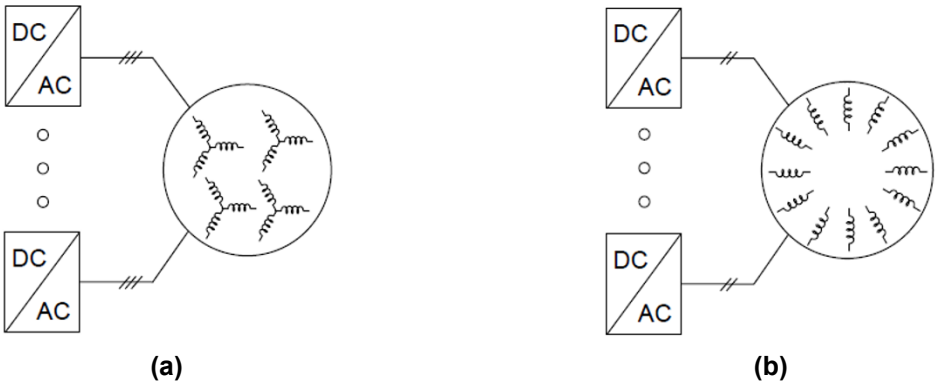


Fig. 1. Two superior structures for the twelve-phase PMSM electric drive: a) Asymmetric 12-phase drive, including four sets of three-phase star-connected windings and four three-phase inverters; b) Symmetric 12-phase drive, including 12 separate open-ended windings and 12 independent single-phase H-bridge inverters [3].

To improve the performance of the PMSM drive under fault conditions, the source of the fault must firstly be identified, and then an appropriate control method should be applied [6]. Therefore, fault diagnosis and fault control are two successive stages. Faults in a drive system can be divided into two categories: mechanical faults and electrical faults. Unfortunately, most mechanical faults, such as bearing faults, are irreversible and unrepairable, and fault detection aims to prevent further damage to the drive system and load. But, fortunately, 90% of faults in drives are electrical faults. Therefore, fault-tolerant control mainly focuses on applying appropriate control methods during the occurrence of electrical faults in the drive system. Electrical faults can be classified into five categories: inverter faults, stator faults, sensor faults, control system faults, and demagnetization faults. Among electrical faults, inverter faults are the most common [7]. Inverter faults include open-circuit faults in

semiconductor switches, short-circuit faults in semiconductor switches, open-circuit faults in one leg, and short-circuit faults in one leg [8]. Fault-tolerant control of PMSM drives typically involves both software and hardware methods. The software method refers to improving the control strategy used after a fault occurrence, while the hardware method usually considers using a fault-tolerant inverter structure instead of the conventional inverter structure so that the drive can continue operating. In practice, both software and hardware methods can be combined to create an optimal fault-tolerant control method. For three-phase PMSMs, various fault-tolerant control methods based on direct torque control, model predictive control, and vector control based on MTPA have been proposed. Additionally, different inverter structures, such as three-leg three-phase inverters, four-leg three-phase inverters, and H-bridge three-phase inverters, have been utilized [9].

To apply appropriate control methods to the twelve-phase PMSM and also control the motor under fault conditions, a suitable dynamic model of the motor must be employed. For dynamic modeling of sinusoidal three-phase PMSMs, Park (dq) or Clarke (αβ) transformations are typically employed to represent the system in either rotating or stationary reference frames. Similarly, for twelve-phase PMSMs, various modeling approaches exist, analogous to those used for three-phase motors. These methods include (1) Modeling in independent $dq$ reference frames [10], (2) Modeling in independent, decoupled $dq$ frames [11], (3) Modeling using vector space decomposition (VSD) [12], and (4) Modeling in twelve-axis stationary reference frame [13]. For a twelve-phase PMSM with sinusoidal back EMF, the first three modeling methods are commonly employed, with no significant difference in computational complexity among them. However, modeling non-sinusoidal PMSMs requires additional consideration when applying these methods. Proposed approaches for modeling non-sinusoidal PMSMs include (a) non-sinusoidal vectorial or extended Park method [14], (b) Modeling in one $dq$ reference frame considering harmonic components [15], (c) Modeling in multiple harmonic $dq$ reference frames (MRF) [16], and (d) Vector space decomposition (VSD) method [28]. The VSD modeling method offers several advantages, including the ability to work with simplified models across three two-dimensional subspaces, facilitating easier controller design and more straightforward harmonic control.

Additionally, this method enables the modeling of non-sinusoidal motors—such as those with non-sinusoidal back-EMF voltages—as sinusoidal motors, simplifying analysis and control. However, both the VSD method and other dq-based modeling techniques are only applicable when the motor employs a centralized control system. Due to the modular structure of the drive system studied in this research, conventional two-axis-based modeling methods cannot be applied. Furthermore, the non-sinusoidal nature of the back-EMF voltages adds to the complexity. Therefore, for the twelve-phase PMSM with double winding, as illustrated in Fig. 2, modeling in the twelve-axis stationary reference frame is required.

This paper studies fault-tolerant control for a twelve-phase PMSM with double stator winding. The physical distribution of the windings of this motor is shown in Fig. 2. The angle between two adjacent phase windings is 15 degrees.

It should be noted that in this motor, there are practically 24 independent single-phase H-bridge inverters and a total of 96 switches, which are controlled by 12 independent microcontrollers. Fig. 3 shows the schematic of the modular drive of the twelve-phase double stator PMSM, where each half of the winding of each phase is powered by a single-phase H-bridge inverter.

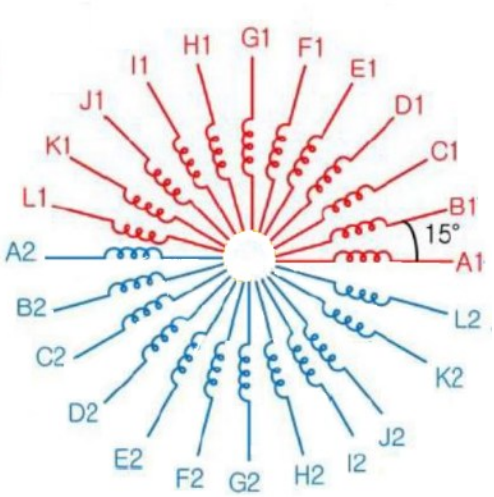


Fig. 2. Winding arrangement in the 12-phase PMSM with double winding used in this research.

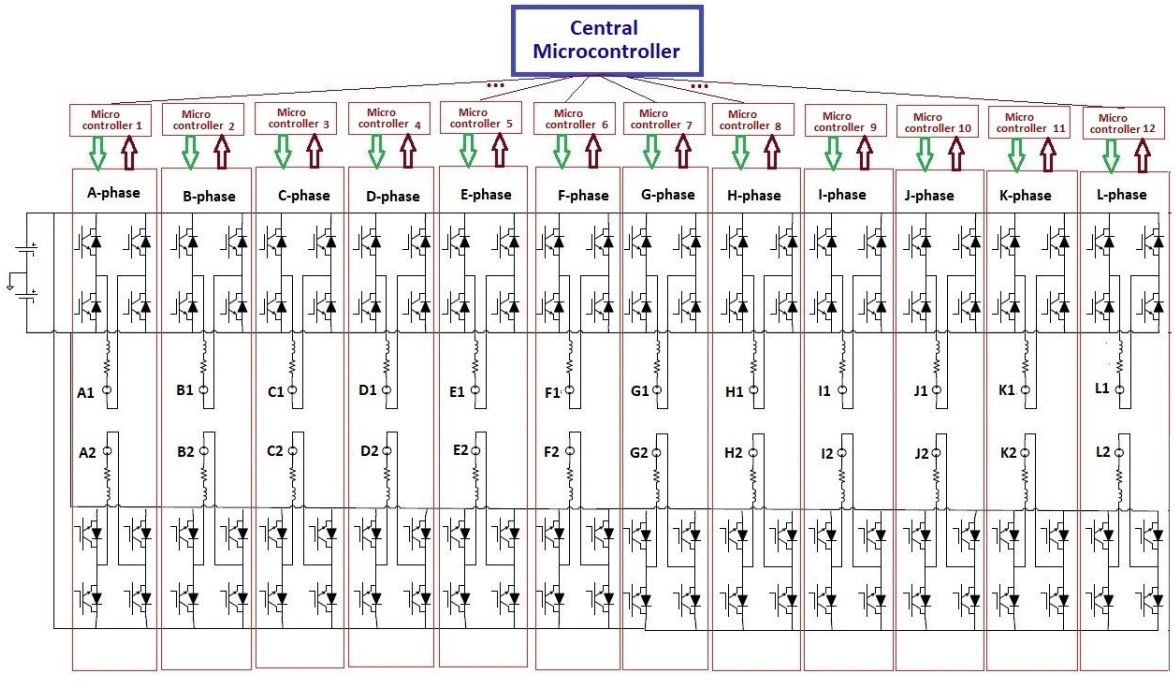


Fig. 3. Schematic of the modular drive system for the 12-phase PMSM with double winding studied in this research.

As shown in Fig. 3, both H-bridge inverters of a phase are controlled by a local microcontroller, and have no data exchange with the other microcontrollers. So, each local microcontroller controls itself windings is unaware of the voltage and current of other phases. A central microcontroller upstream of all local microcontroller receives the reference and actual values of speed, rotor position and health status of each module (including winding and H-bridge inverter) and then determines the reference currents of each phase and send to the corresponding local microcontroller.

The control methods for three-phase PMSMs are highly diverse. While these methods can also be applied to twelve-phase PMSMs, their practical use is less common due to the increased number of phases, higher computational burden, processing limitations in microcontrollers, and the poor performance of some methods in high-power motors. Vector

control is the most widely used primary method for both three-phase and twelve-phase PMSMs, offering relatively fast dynamics and smoother torque compared to other approaches [17]. For twelve-phase PMSMs, vector control is implemented in independent dq frames, decoupled dq frames method [18]. However, vector control for twelve-phase PMSMs has several drawbacks, including the computational complexity of Park transformations, challenges in tuning multiple PI controller coefficients, and sensitivity to changes in motor parameters. Model Predictive Control (MPC) has emerged as an effective and optimal strategy for controlling switching and nonlinear systems, gaining widespread adoption in electric drive applications, including PMSM drives [19]. Several studies have explored MPC for twelve-phase PMSMs using two-level [20,21]. However, MPC is also sensitive to parameter variations, and while model-free and robust predictive methods have been proposed for three-phase PMSMs, they have not yet been extended to twelve-phase PMSMs. Most conventional control methods rely on motor models in two-axis reference frames, necessitating transformations such as abc-to-dq or αβ. However, in the modular drive structure investigated in this research—where each phase is controlled independently—these conventional methods cannot be applied. In summary, due to the modular architecture of the control system studied here, none of the existing modeling and control methods based on two-axis theory (for either three-phase or twelve-phase PMSMs) are suitable. Instead, phase-independent modeling and control approaches must be developed.

The rest of this paper is organized as follows. In section 2, firstly the motor modeling in twelve-axis stationary reference frames is presented, and then, considering the non-sinusoidal back-EMF voltages, drive control using the harmonic current injection strategy is developed with respect to the modular system limitations. Section 3 presents a fault-tolerant control based on zeroing the resultant torque resulting from the second harmonic of the remaining healthy windings under various fault conditions. In section 4, to demonstrate the theoretical analysis, some simulation results of the drive performance at healthy and faulty conditions are provided and in section 5 some experimental results are provided. Finally in section 6, the conclusion and some suggestions are presented.

## 2. MODELING AND CONTROL OF MODULAR DOUBLE-WINDING TWELVE-PHASE PMSM

### 2.1. Modeling in Stationery Reference Frame

Due to the modular nature of the motor and control system, as shown in Fig. 3, there is no data exchange between the control systems of the motor phases. Therefore, none of the three-phase and twelve-phase PMSM modeling methods based on the two-axis theory and control methods for symmetric twelve-phase PMSMs cannot be applied. Additionally, the non-sinusoidal nature of the back-EMF voltages further complicates it. Fig. 4 shows the detailed data exchange between central microcontroller and local microcontrollers.

Therefore, for the twelve-phase modular motor with non-sinusoidal back EMF voltages, modeling must be performed in a twelve-axis stationary frame. Using arrangement of the PMSM windings shown in Fig. 2, the voltage-current relationship for each phase obeys the following:

$$v_x = R_s i_x + \frac{d}{dt}\psi_x + e_x \quad (1)$$

where $R_s$ is the resistance of each phase, and $v_x$, $i_x$, $e_x$ are the voltage, current, induced back-EMF voltage due to the permanent magnet of the rotor and $\psi_x$ is the flux linkage of the winding $x$, $(x = A_1, A_2, B_1, \dots, L_2)$ respectively. The flux linkage of each winding depends on the its own current and the current of the other 23 windings and can be calculated using the following relation:

$$\psi_x = L_x i_x + \sum_{\substack{y=A_1,A_2,B_1,B_2,\dots,L_2 \\ (x \neq y)}} M_{xy} i_y \quad (2)$$

where $L_x$ and $M_{xy}$ are the self-inductance of winding $x$ and the mutual inductance between two windings $x$ and $y$. The stator inductance matrix, when two windings of each phase $(eg.\ A_1, A_2)$ are separate, is a $24 \times 24$ matrix. But for improvement the motor performance at low speeds, two windings of a phase are connected in series and so, the inductance matrix is converted to a 12× 12 matrix. Supposing that the PMSM in this study has a surface-mounted rotor type, the stator inductance matrix always has constant elements. The electromagnetic torque of the double-winding twelve-phase motor $T_e$ and the mechanical speed of the motor $\omega_m$ can also be calculated using the following relations:

$$T_e = \sum_{x=A_1,\dots,L_2} \frac{e_x i_x}{\omega_r} \quad (3)$$

$$\omega_m = \frac{1}{J} \int (T_e - T_l) dt \quad (4)$$

where $\omega_r$, $J$, and $T_l$ are the electrical rotor speed, rotor inertia moment, and load torque, respectively. To implement of the model in Simulink, a 24-phase winding can be used, that to each phase, a dependent voltage source with desired harmonic waveform function of rotor position $\theta_r$ and amplitude as function of rotor speed, can be added in series.

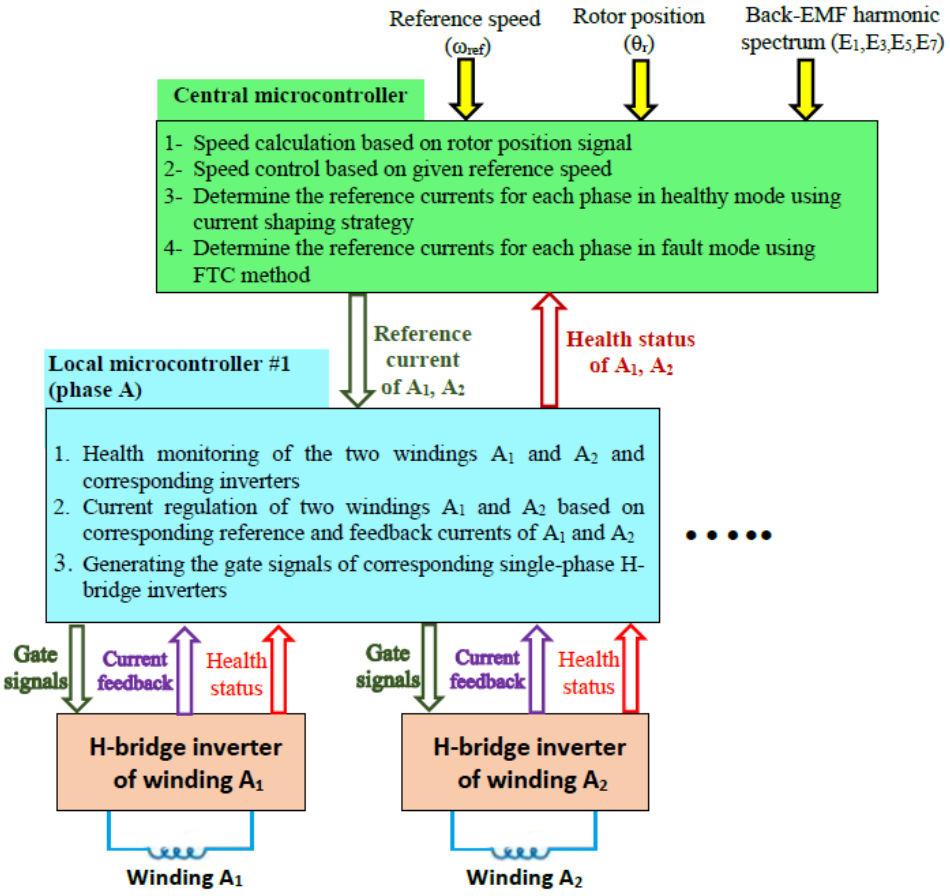


Fig. 4. Flowchart of data exchange between micro-controllers in the modular drive of twelve-phase PMSM studied in this research.

## 2.2. Control using Harmonic Current Injection Strategy

Due to the harmonics present in the back EMF voltages of the phases, the harmonic current injection strategy in stationery reference frame is used to reduce the torque ripple of the motor. In this strategy, harmonic currents with appropriate amplitudes are adjusted in each phase so that the harmonic components of the torque are nullified and only the constant torque remains [22]. For the motor studied in this paper, only the 1st, 3rd, 5th, and 7th harmonics are present in the back EMF voltages of each phase; So, back EMF voltage of winding $x$ (here; $x = A_1, A_2$) can be written as follows:

$$e_x(t) = E_1 \sin \omega_r t + E_3 \sin 3\,\omega_r t + E_5 \sin 5\,\omega_r t + E_7 \sin 7\,\omega_r t \quad (5)$$

where $E_1$ to $E_7$ are the amplitudes of the back-EMF voltage harmonics, that are 1, 0.2, 0.1, and 0.02 per unit, respectively. If the injected current into winding $x$ (here; $x = A_1, A_2$) is considered as:

$$i_x(t) = I_1 \sin \omega_r t + I_5 \sin 5\,\omega_r t + I_7 \sin 7\,\omega_r t \quad (6)$$

where $I_1$ to $I_7$ are the amplitudes of the phase currents' harmonics. Note that for other windings, the argument of the sinusoidal functions in above equations changes according to Fig. 2. For example, for windings of two phases $B$ and $L$, they can be written as:

$$i_{B_1}(t) = i_{B_2}(t) = I_1 sin(\omega_r t + 15^o) + I_5 sin5(\omega_r t + 15^o) + I_7 sin7(\omega_r t + 15^o) \quad (7)$$

$$i_{L_1}(t) = i_{L_2}(t) = I_1 sin(\omega_r t + 165^o) + I_5 sin5(\omega_r t + 165^o) + I_7 sin7(\omega_r t + 165^o) \quad (8)$$

With some calculations, it can be shown that the total instantaneous air gap electromagnetic torque ($T_e$) of the motor studied in this paper with Eqs. (5)-(6) can be calculated as follows:

$$T_e(t) = \frac{P_e(t)}{\omega_r} = \frac{\sum e_x(t) i_x(t)}{\omega_r} = T_0 + T_6 \sin 6\omega_r t + T_{12} \sin 12\,\omega_r t \quad (9)$$

where, $P_e$ is the airgap power of the motor and $T_0$, $T_6$ and $T_{12}$ are the average torque component and the 6th and 12th order harmonics of the instantaneous motor torque, respectively and are derived as follow:

$$T_0 = \frac{3}{2\omega_r}[E_1 I_1 + E_5 I_5 + E_7 I_7] \quad (10)$$

$$T_6 = \frac{3}{2\omega_r}[I_1(E_7 - E_5) - I_5 E_1 + I_7 E_1] \quad (11)$$

$$T_{12} = \frac{3}{2\omega_r}[-I_5 E_7 - I_7 E_5] \quad (12)$$

To determine the amplitude values of the harmonic currents for each phase, by setting $T_0$ equal to the reference torque ($T_e^*$; output of the speed controller) and setting $T_6$ and $T_{12}$ to zero, the reference values of the harmonic current amplitudes are determined as follows:

$$\begin{bmatrix} I_1^* \\ I_5^* \\ I_7^* \end{bmatrix} = \begin{bmatrix} 1.006 \\ -0.0671 \\ 0.0134 \end{bmatrix} \frac{2\omega_r T_e^*}{3} \quad (13)$$

where $\boldsymbol{I_1^*}$ to $\boldsymbol{I_7^*}$ are the amplitudes of the phase currents' harmonics. Using Eqs. (6) and (13), the time domain of the reference current for both windings of the phase A, based on the reference torque, can be determined as follows:

$$i_{A_1}^*(t) = i_{A_2}^*(t) = I_1^* sin\ \omega_r t + I_5^* sin\ 5\omega_r t + I_7^* sin\ 7\omega_r t \quad (14)$$

Tracking the harmonic reference current proposed with Eq. (6) using conventional PI controllers, with respect to their limited bandwidth, does not yield a satisfactory dynamic response and results in significant torque ripple. Hysteresis controllers also do not provide satisfactory responses for current regulation due to variable switching frequencies and

permanent current errors. In contrast, proportional-resonant (PR) controllers have higher gain at the resonant frequency, which can be used to track AC reference signals with frequency equal to the resonance frequency [16]. However, the high gain at the resonant frequency makes the system sensitive to external signal frequencies, leading to instability. Therefore, a quasi-PR (QPR) controller has been proposed, which not only maintains the ability to control AC signals like a PR controller but also increases the bandwidth of high gain. The transfer function of the QPR controller can be expressed as follows:

$$G_{QPR}(s) = K_P + K_R \frac{2\omega_c s}{s^2+2\omega_c s+\omega_o^2} \quad (15)$$

where $\omega_0$ is the resonant frequency, $K_p$ and $K_R$ are the proportional gain and resonant gain, respectively, and $\omega_c$ is the cut-off frequency of the transfer function. If, in addition to controlling the main signal with frequency $\omega_0$, the reference signal includes higher order harmonic signals, it is needed to modify transfer function Eq. (15) with respect to existence harmonics. Hence, with respect to the reference current shown by Eq. (6), the transfer function of the QPR controller should be considered as follows:

$$G_{QPR}(s) = K_P + K_{R_1} \frac{2\omega_{c_1} s}{s^2+2\omega_{c_1} s+(\omega_o)^2} + K_{R_5} \frac{2\omega_{c_5} s}{s^2+2\omega_{c_5} s+(5\omega_o)^2} + K_{R_7} \frac{2\omega_{c_7} s}{s^2+2\omega_{c_7} s+(7\omega_o)^2} \quad (16)$$

where $K_{Rh}$ is the resonant gain corresponding to h$^{th}$ harmonic (h = 1,5,7), $\omega_{c_h}$ is the cut-off frequency due to h$^{th}$ harmonic [23]. The optimal values of the parameters $K_P$, $K_{Rh}$, and $\omega_{Ch}$ for the twelve-phase PMSM drive in this research and for its different harmonics are determined using the trial-and-error method [22].

## 3. FAULT-TOLERANT CONTROL IN MODULAR TWELVE-PHASE PMSM DRIVE

Significant work has been done over the past two decades on fault-tolerant control for multiphase PMSMs with fewer than 12 phases, including five-phase and asymmetric twelve-phase motors [24,25]. However, only limited research has been conducted on twelve-phase PMSMs and brushless DC (BLDC) motors. In reference [26], a fault-tolerant control method for a twelve-phase PMSM connected to a mechanical flywheel load is presented for an open-circuit fault in one phase of the motor. In the drive structure presented in this reference, the twelve-phase motor is considered as four three-phase motors, with each three-phase set modeled independently in the $dq$ reference frame that each set powered by an independent three-phase three-level inverter. Ref. [27] extends the method presented in reference [26] for the same twelve-phase PMSM by proposing a fault-tolerant control method for two open-circuit faults in two different three-phase sets. In the proposed method, the two faulty three-phase sets are considered as two single-phase motors. In [14], a fault-tolerant control method is provided for a twelve-phase BLDC motor powered by 12 independent single-phase H-bridge inverters in the case of an open-circuit fault in one phase. In the proposed FTC method, assuming sinusoidal shape for currents and back EMF voltages, with the occurrence of a fault and the loss of one or more phases, the total electromagnetic torque includes the constant torque as well as harmonic oscillations with twice the current frequency. In proposed FTC, the amplitude and phase of the current in some healthy phases are adjusted such that the sum of the second-order harmonic components of torque of all remaining healthy phases becomes zero.

The fault-tolerant control strategy used in this study is based on balancing the second harmonic components of the torque in the motor windings under fault conditions. In a healthy state, the second harmonic components of the motor phase torque are balanced with each

other, resulting in a sum of zero. Consequently, the instantaneous torque of the motor, with ignoring the effects of the non-sinusoidal back-EMF voltages, cogging torque, and high-frequency oscillations due to inverter switching, remains constant.

However, when a fault occurs in one or more windings, the generated torque becomes oscillatory, adding a second harmonic oscillatory torque component to the constant torque. The fault-tolerant control (FTC) strategy used in this study is based on reconstructing the amplitude and angle of the main harmonic current of one or some healthy windings to re-establish the balance between the second harmonic torques of the healthy winding [5]. Suppose the main harmonic current vectors of the twelve motor phases are shown in Fig. 5(a). The second harmonic torque component vectors of the various phases will be as depicted in Fig. 5(b), which are in complete balance with each other and sum is zero.

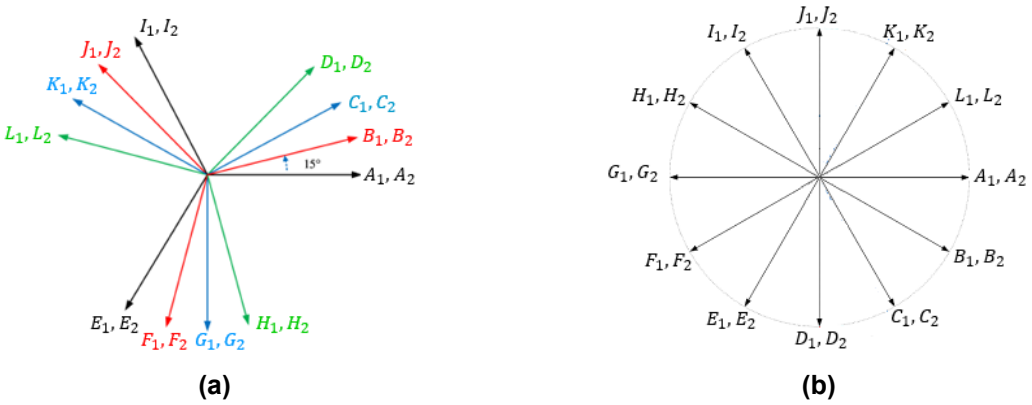


Fig. 5. Current vectors and second harmonic torque vectors of the windings of the twelve-phase PMSM: a) Main harmonic current vectors; b) Second harmonic torque component vectors.

### 3.1. Single-Phase Fault

With an open-circuit fault in the winding $A_1$ of phase $A$, a non-zero second harmonic appeared in the total torque. In other words, in Fig. 6, by removing the second harmonic vector of the winding $A_1$ (dashed vector), the sum of the second harmonic torque vectors of the remaining 11 healthy phases is no longer zero. To eliminate the second harmonic of the torque in the fault condition, two vectors $E_1$ and $I_1$ to be shifted by $\theta_{shift}$ toward the lost winding $A_1$ to obtain the new torque vectors $E'_1$ and $I'_1$. This shift must be such that the sum of the second harmonic torque component vectors of the remaining phases becomes zero.

According to Fig. 6, the necessary second harmonic torque component angle shift for two windings $E_1$ and $I_1$ are $-30^o$ and $+30^o$. Note that these $30^o$ shifts occur in the second harmonic torque of these two windings. Since the torque angle of each phase is the sum of the current angle and the back-EMF voltage angle, and the back- EMF voltage angle cannot be changed, to change the angle of torque, the main harmonic current angle of corresponding phase must be shifted by exactly $30^o$.

Also, the amplitudes of all windings are adjusted to appropriate and permissible values to meet the load torque requirements. In each set of 12 windings, there are 12 single-phase fault scenarios, which are listed in Table 1 along with their compensator phases. For faults in the second winding of each phase (e.g., a fault in $A_2$), the same Table can be used, and the last row in Table 1 refers to compensating for a fault in the winding $A_2$. In total, there are 24 single-phase fault scenarios.

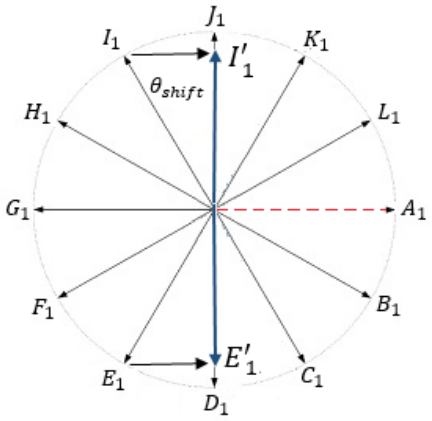


Fig. 6. Second harmonic torque angle shift of the two windings $\boldsymbol{E_1}$, $\boldsymbol{I_1}$ in twelve-phase PMSM in the case of fault in winding $\boldsymbol{A_1}$.

Table 1. Single-phase fault scenarios and corresponding compensator windings (In total 24 scenarios).

| Faulty winding | Compensator windings | | Required angle shift in compensator windings | |
|---|---|---|---|---|
| $A_1$ | $I_1$ | $E_1$ | $+30^o$ | $-30^o$ |
| $B_1$ | $-$ | $F_1$ | $-$ | $-60^o$ |
| $C_1$ | $K_1$ | $-$ | $+60^o$ | $-$ |
| $D_1$ | $L_1$ | $H_1$ | $+30^o$ | $-30^o$ |
| $E_1$ | $-$ | $I_1$ | $-$ | $-60^o$ |
| $F_1$ | $B_1$ | $-$ | $+60^o$ | $-$ |
| $G_1$ | $C_1$ | $K_1$ | $+30^o$ | $-30^o$ |
| $H_1$ | $-$ | $L_1$ | $-$ | $-60^o$ |
| $I_1$ | $E_1$ | $-$ | $+60^o$ | $-$ |
| $J_1$ | $F_1$ | $B_1$ | $+30^o$ | $-30^o$ |
| $K_1$ | $-$ | $C_1$ | $-$ | $-60^o$ |
| $L_1$ | $H_1$ | $-$ | $+60^o$ | $-$ |
| $A_2$ | $I_2$ | $E_2$ | $+30^o$ | $-30^o$ |

### 3.2. Two-Phase Fault

Suppose that two windings $A_1$ and $B_1$ have a fault. In this case, according to Fig. 5, there are two balanced three-phase sets $(C_1, G_1, K_1)$ and $(D_1, H_1, L_1)$ where the sum of the second harmonic torques of each set is zero. However, the three-phase set $(A_1, E_1, I_1)$ becomes unbalanced due to loss of winding $A_1$ and the three-phase set $(B_1, F_1, J_1)$ becomes unbalanced due to loss of winding $B_1$. To compensate for these faults, with similar manner to single-phase fault compensation, the current angle of the two windings $(E_1, I_1)$ is shifted by $(-30°, +30°)$ to compensate for the lost $A_1$ winding, and the current angle of the two windings $(F_1, J_1)$ is shifted by $(-60°, 0°)$ to compensate for the lost winding $B_1$. In each set of 12 windings, the number of two-phase fault scenarios is equal to the function $\binom{12}{2}$, which is 66 cases, that some of them are listed in Table 2 and there are totally 122 two-phase fault scenarios. Note that if two faults occur in two windings belonged to different sets (for example, $A_1$ and $B_2$), the single-phase fault analysis method described in sections 3.1 is used for each set.

### 3.3. Three-Phase Fault

In the event of fault in three phases, the compensation is carried out similarly to the previous two cases. In this case and for each set of 12 windings, the number of three-phase

fault scenarios is equal to the function $\binom{12}{3}$, which is 220 cases, that two cases of them are listed in Table 3 and there are totally 440 three-phase fault scenarios. Note that if three faults occur in two different sets (in a 2+1 manner), compensation method described for single-phase and two-phase faults in 3.1 and 3.2 should be used.

Table 2. Some two-phase fault scenarios and corresponding compensator windings (In total 122 scenarios).

| Faulty windings | Compensator windings | | | | Required angle shift in compensator windings | | | |
|---|---|---|---|---|---|---|---|---|
| $A_1, B_1$ | $I_1$ | $E_1$ | $K_1$ | $F_1$ | $+30^o$ | $-30^o$ | $0^o$ | $-60^o$ |
| $A_1, C_1$ | $I_1$ | $E_1$ | $K_1$ | $-$ | $+30^o$ | $-30^o$ | $+60^o$ | $0^o$ |
| $A_1, D_1$ | $I_1$ | $E_1$ | $L_1$ | $H_1$ | $+30^o$ | $-30^o$ | $+30^o$ | $-30^o$ |
| $A_1, E_1$ | $-$ | $G_1$ | $-$ | $-$ | $0^o$ | $-60^o$ | $0^o$ | $0^o$ |
| $A_1, F_1$ | $I_1$ | $E_1$ | $B_1$ | $-$ | $+30^o$ | $-30^o$ | $+60^o$ | $0^o$ |
| $A_1, G_1$ | $I_1$ | $E_1$ | $C_1$ | $K_1$ | $+30^o$ | $-30^o$ | $+30^o$ | $-30^o$ |
| $A_1, H_1$ | $I_1$ | $E_1$ | $-$ | $L_1$ | $+30^o$ | $-30^o$ | $0^o$ | $-60^o$ |
| $A_1, I_1$ | $G_1$ | $-$ | $-$ | $-$ | $+60^o$ | $0^o$ | $0^o$ | $0^o$ |
| $A_1, J_1$ | $I_1$ | $E_1$ | $F_1$ | $B_1$ | $+30^o$ | $-30^o$ | $+30^o$ | $-30^o$ |
| $A_1, K_1$ | $I_1$ | $E_1$ | $-$ | $C_1$ | $+30^o$ | $-30^o$ | $0^o$ | $-60^o$ |
| $A_1, L_1$ | $I_1$ | $E_1$ | $H_1$ | $-$ | $+30^o$ | $-30^o$ | $+60^o$ | $0^o$ |

Table 3. Some three-phase fault scenarios and corresponding compensator windings (In total 440 scenarios).

| Faulty windings | Compensator windings | Required angle shift in compensator windings |
|---|---|---|
| $A_1, B_1, C_1$ | $I_1, E_1, F_1, K_1$ | $+30^o, -30^o, -60^o, +60^o$ |
| $A_1, B_1, D_1$ | $I_1, E_1, F_1, L_1, H_1$ | $+30^o, -30^o, -60^o, +60^o, -30^o$ |

### 3.4. Four-Phase Fault and More

In the event of fault in four phases, the compensation is again carried out similarly to the previous cases. However, in this case, the number of compensator windings increases, and in some cases, it may reach up to 8 windings. In this case and for each set of 12 windings, the number of four-phase fault scenarios is equal to the function $\binom{12}{4}$, which is 495 cases, that two cases of them are listed in Table 4 and there are totally 990 four-phase fault scenarios. Note that if the faults occur in two different sets, depending on the combination of the fault in two sets (1+3 or 2+2), the compensation method described in the three sections 3.1 to 3.3 are used. For fault occurrences in five phases and more, a similar approach can be applied, but for brevity, the fault occurrences in five phases and more are not discussed.

Table 4. Some four-phase fault scenarios and corresponding compensator windings (In total 990 scenarios).

| Faulty windings | Compensator windings | Required angle shift in compensator windings |
|---|---|---|
| $A_1, B_1, C_1, D_1$ | $I_1, E_1, F_1, K_1, L_1, H_1$ | $+30^o, -30^o, -60^o, +60^o, +30^o, -30^o$ |
| $A_1, B_1, D_1, E_1$ | $G_1, H_1$ | $-60^o, -150^o$ |

## 4. SIMULATION RESULTS

In this section, for a twelve-phase 10-pole motor with nominal specifications of 200 kW power, 320 V voltage, 315 rpm speed, 15 mΩ phase resistance, 525 μH phase inductance, 0.15

Kg.m² inertia, 1.2 Wb pole flux, and 25.5 $N.m/A$ torque constant, some simulations are presented. Fig. 7 illustrates the block diagram of the double stator winding, twelve-phase PMSM control system in this study using harmonic current injection strategy as well as QPR controllers for winding current regulation. A PI controller generates reference torque based on tracking error of speed. Using harmonic current injection strategy and based on eq. (14) the current reference for all phases is determined and finally by 24 QPR controllers, the current regulation is implemented.

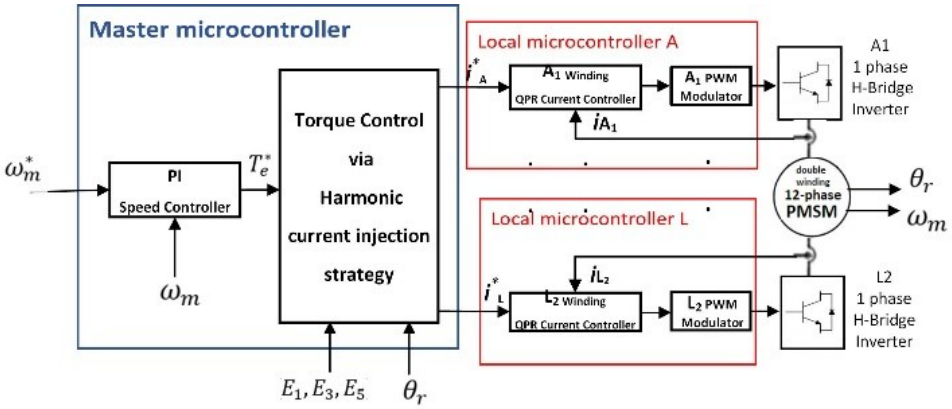


Fig. 7. Schematic of control system for the double stator windings twelve-phase PMSM using harmonic current injection strategy.

In this section, four fault scenarios are simulated that faulty windings are belonged to one set of 12-windings. To simulate the performance of the fault-tolerant control system in a single-phase fault, it is assumed that the winding $A_1$ of phase A is lost at time t=0.65 sec. To observe the disturbance in the developed electromagnetic torque, it is assumed that the fault-tolerant control (FTC) algorithm is activated after 0.2 sec delay at t=0.85 sec. According to Table 1 it is carried out by adjusting the amplitude and angle of the two windings $E_1$ and $I_1$. Fig. 8 shows the simulation results that the torque experiences some oscillations.

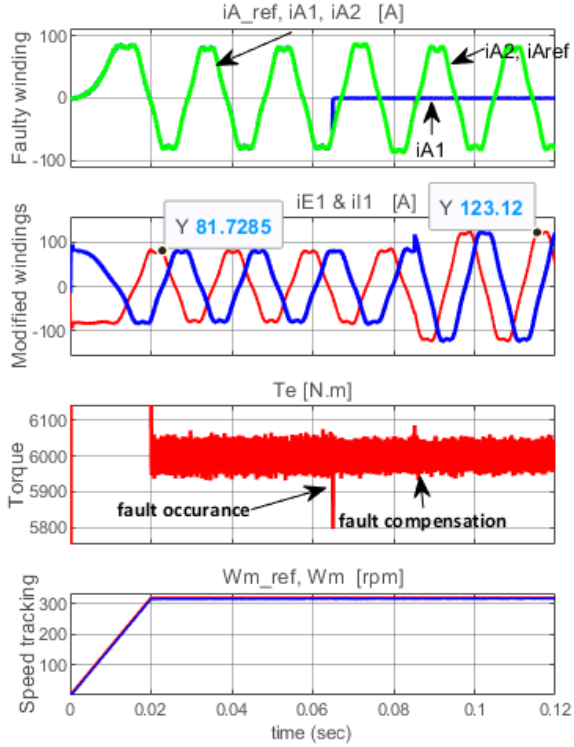


Fig. 8. Behaviour of the fault-tolerant control system in the event of the single-phase fault in windings $\boldsymbol{A_1}$.

Although this oscillation is not very noticeable due to the many numbers of healthy windings, even this slight oscillation is eliminated by applying the fault-tolerant control method. According to the first row of Table 1, to compensate for the fault, the current angles of the two windings $E_1$ and $I_1$ are changed by (-30°, +30°) and the reference current value of the compensating windings $E_1$ and $I_1$ is increased by 50%, from 81 A to 123 A. Fig. 9 shows the system's performance simulation under two-winding fault conditions.

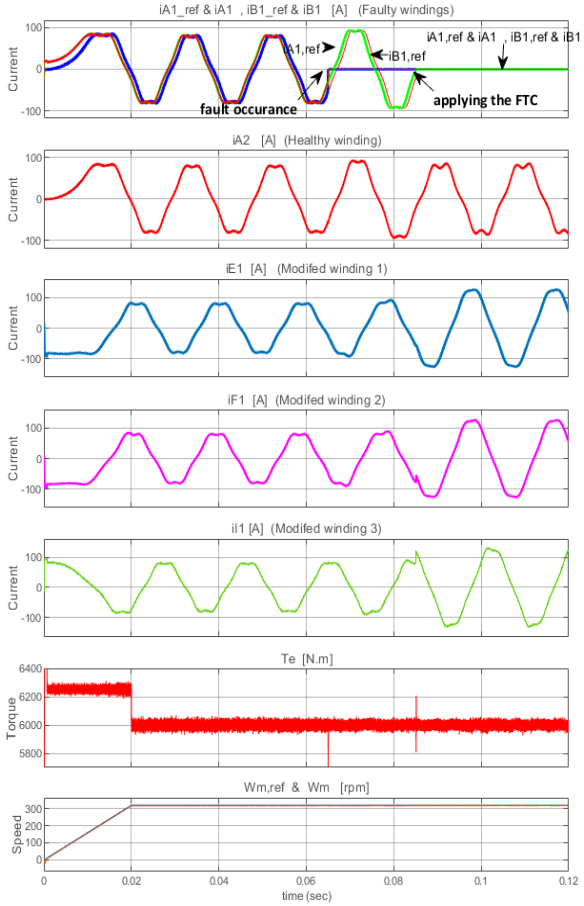


Fig. 9. Behaviour of the fault-tolerant control system in the event of the two-phase fault in windings $\boldsymbol{A_1}$ and $\boldsymbol{B_1}$.

The two windings $A_1$ and $B_1$ are lost at time t = 0.65 sec, and to compensate for this, according to the first row of Table 2, the current angles of the three windings $E_1$, $F_1$ and $I_1$ are changed to (-30°, -60°, +30°), and their amplitudes are increased by 50%. Upon the occurrence of the fault, the torque experiences slight oscillations; however, after applying the fault-tolerant control method at t = 0.85 sec, the quality of the produced torque returns to the state before the fault occurred. Fig. 10 shows the system's performance simulation under a load torque of 6000 $N \cdot m$ in the event of the fault in three windings. The three windings $A_1$, $B_1$ and $C_1$ are lost at time t = 0.65 sec, and to compensate for this, according to the first row of Table 3, the reference values' amplitude is increased by 50%, from 80 A to 126 A. Upon the occurrence of the fault, the torque experiences severe oscillations, and the speed even drops from 316 rpm to 260 rpm. After applying the fault-tolerant control method at t = 0.85 sec, the torque and speed return to the state before the fault occurrence. Fig. 11 shows the system's performance simulation under a load torque of 6000 $N \cdot m$ in the event of the fault in four windings. The four windings $A_1$, $B_1$, $C_1$ and $D_1$ are lost at time t = 0.65 sec, and to compensate for this, according to the first row of Table 4, the reference values' amplitude is increased by 50%. Upon the occurrence of the fault, the torque is significantly reduced, and the speed also experiences

a noticeable drop. After applying the fault-tolerant control method at t = 0.85 sec, the produced torque and speed tracking return to the state before the fault occurred.

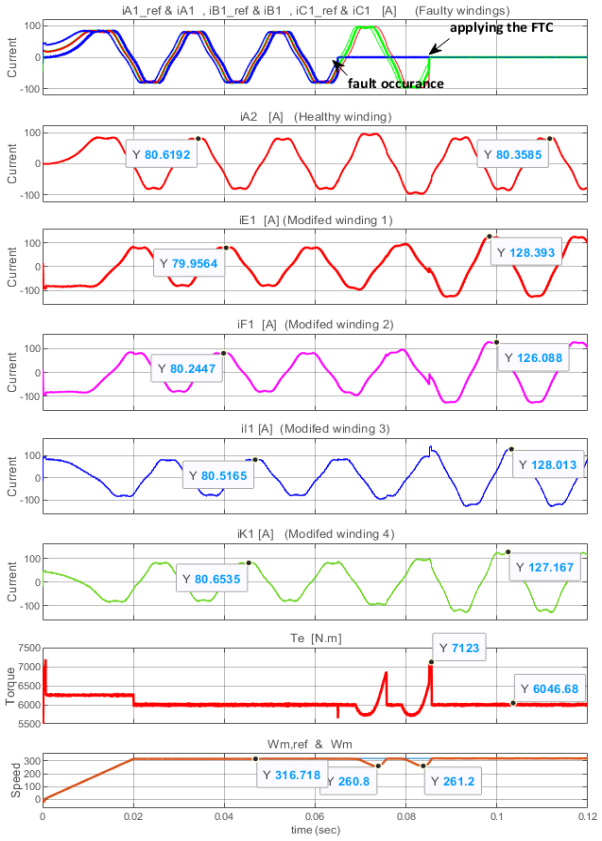


Fig. 10. Behaviour of the fault-tolerant control system during the three-phase fault in the three windings $\boldsymbol{A_1}$, $\boldsymbol{B_1}$ and $\boldsymbol{C_1}$.

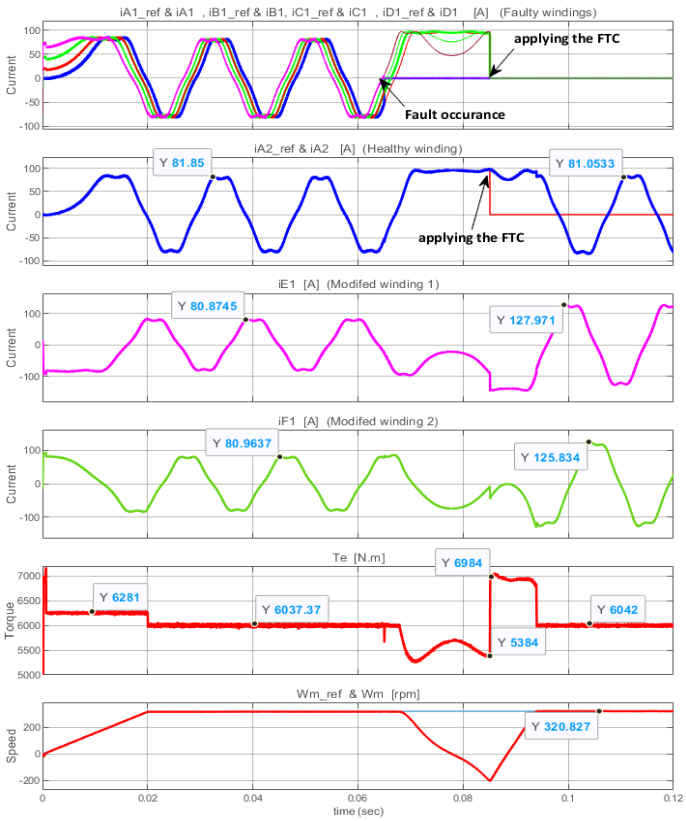


Fig. 11. Behaviour of the fault-tolerant control system in the event of the four-phase fault in the four windings $\boldsymbol{A_1}$, $\boldsymbol{B_1}$, $\boldsymbol{C_1}$ and $\boldsymbol{D_1}$.

## 5. EXPERIMENTAL RESULTS

To confirm the proposed FTC control methods in fault conditions for the double-winding twelve-phase PMSM drive, some practical tests were conducted on the laboratory setup using introduced PMSM in previous section. The schematic of the setup is shown in Fig. 12, where 13 STM32F407VGT6 microcontrollers have been used as central and local controllers. The drive of each phase consists of a microcontroller board as well as double H-bridge single-phase inverters and a separate excited DC generator is employed as load. The parameters for all winding QPR controllers are the same and, according to (17), are $K_P$ = 1, $K_{R1}$ = 15, $K_{R3}$ = 0.1, $K_{R5}$ = 0.1, and $\omega_{ci}$ = 10.

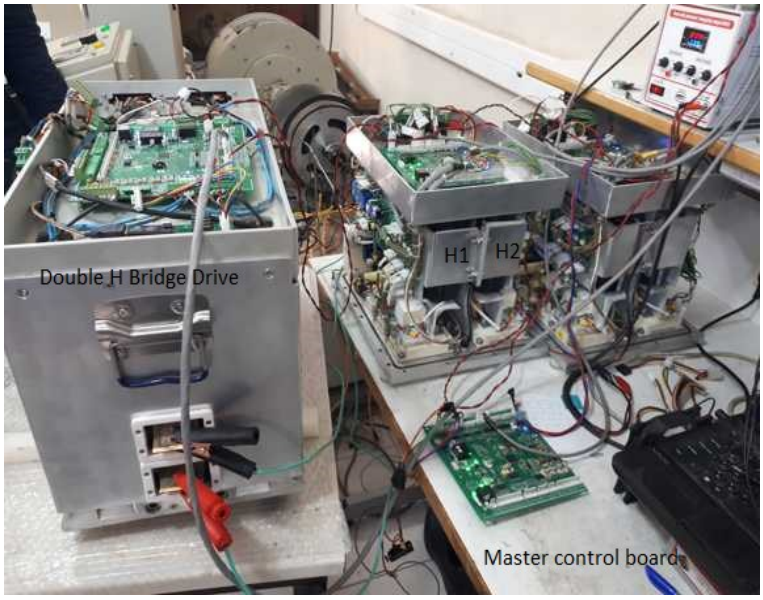


Fig. 12. Experimental setup of modular twelve-phase PMSM drive.

The practical test results for the four-phase fault in windings $A_1, A_2$ and $C_1, C_2$ are examined. For this purpose, the dual H-bridge inverters of two modules A ($H_1$) and C ($H_3$) are turned off. Actually, this case of fault is a two-phase fault in two different sets corresponding to the second row of Table 2. Fig 13 shows the motor speed and winding current $I_1$ in healthy condition of the motor at speed reference or 120 rpm, whereas harmonic current injection strategy is employed. The speed fluctuation is 3 rpm (about 2.5%). Fig 14(a) shows the motor speed and winding current $I_1$ while two modules A and C are turned off and four windings $A_1, A_2$ and $C_1, C_2$ have no involvement to develop the torque. It can be seen that due to the torque ripple created, the speed fluctuation increases to 12 rpm (about 10%). To reduce torque ripple, the fault tolerant method is used for twelve-phase sets separately. To re-establish balance between 10 remaining vectors in each set, corresponding to the second row of Table 2, the direction of $I_1$ and $E_1$ is shifted by +30° and -30°, resulting in the new current vector $I'_1$ and $E'_1$. Similar compensation is carried out in other 12-winding set and the direction of $I_2$ and $E_2$ is shifted by +30° and -30°. Fig. 13 shows the practical results of applying the proposed FTC method. In Fig 14(b) the motor speed and winding current $I_1$ are shown. The speed fluctuation decreases to 4 rpm, which means 75% improvement in speed fluctuations. Fig. 15 shows the currents of some healthy windings of set 1 ($E_1, I_1, K_1, G_1$). The currents of set 2 ($E_2, I_2, K_2, G_2$) are also identical to the corresponding currents in set 1. When one or more windings are lost, the motor operates unbalanced, which increases the motor vibrations. Considering that in the practical test, ripple measurements were performed based on speed fluctuations, in order to verify the results of torque ripple reduction, vibration measurement was performed by

installing vibration sensors on the motor, gearbox, shaft and load assembly in scenario of four-phase fault in $A_1, A_2$ and $C_1, C_2$.

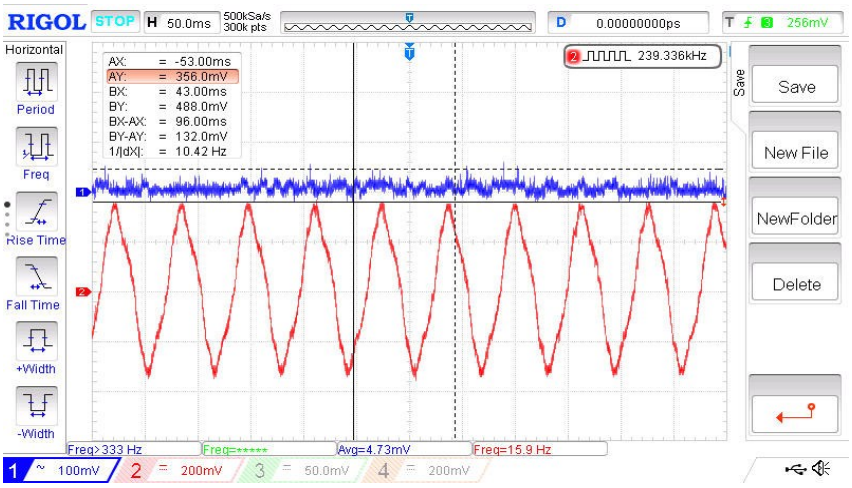


Fig. 13. Behavior of the PMSM drive during in healthy condition (speed: blue waveform, current $I_1$: red).

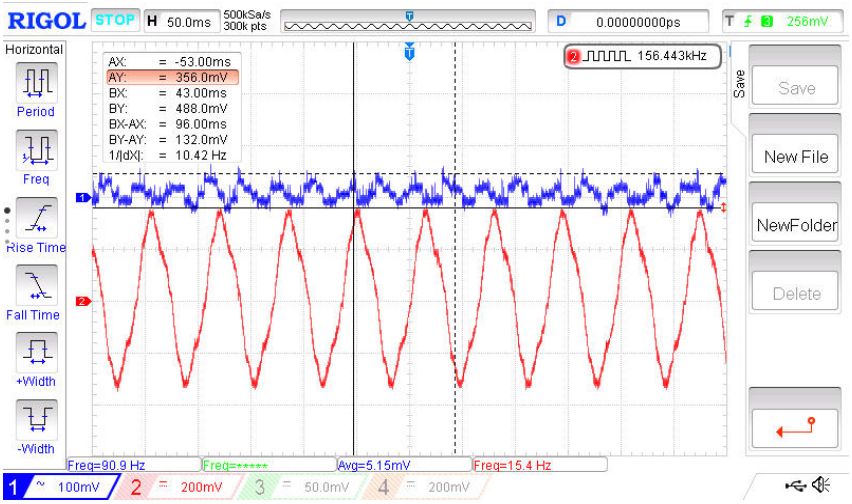


**(a)**

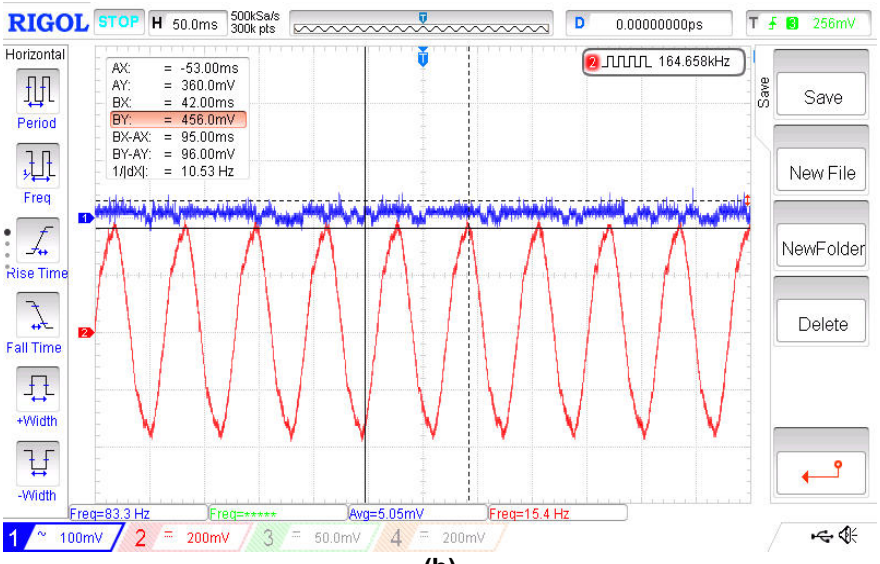


**(b)**

Fig. 14. Behavior of the PMSM drive during four-phase fault on windings $A_1, A_2$ and $C_1, C_2$ (speed: blue waveform, current $I_1$: red): a) without compensation; b) with compensation.

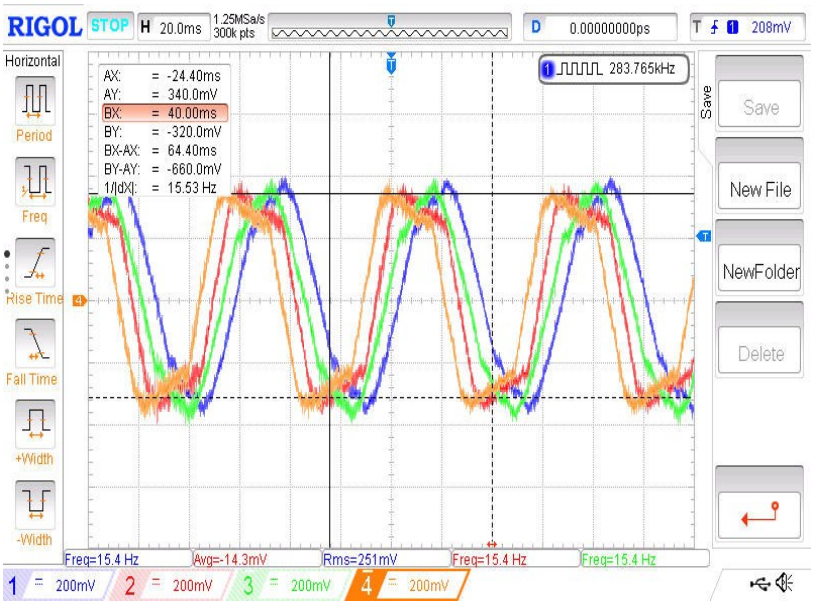


Fig. 15. The current of four windings $E_1, I_1, K_1, G_1$ during four-phase fault on windings $A_1, A_2$ and $C_1, C_2$ by adjusting the angle of current in $I_1, E_1$ and $I_2, E_2$.

Fig. 16 shows the vibration measurement in both cases without compensation and with compensation. It is clear that with using of FTC method, the vibration has decreased significantly.

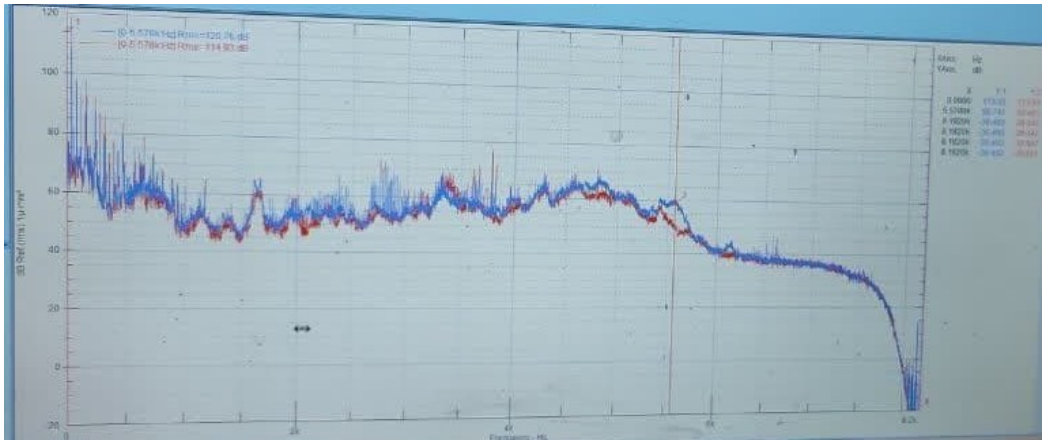

Fig. 16. Vibration measurement in four-phase fault on windings $A_1, A_2$ and $C_1, C_2$ with (red curve) and without compensation (blue curve).

## 6. CONCLUSION

In this paper, fault-tolerant control in the modular twelve-phase PMSM drive has been studied. Considering the non-sinusoidal back-EMF voltage of the motor phases, current shaping or harmonic current injection (HCI) strategy along with QPR current controllers has been used to eliminate second harmonics present in the torque in the healthy state. A fault-tolerant control method in faulty conditions based on elimination the sum of the second harmonic components torque of healthy phases has been presented, and various fault scenarios have been investigated. It is noted the proposed current angle shifts in each fault scenario are not the only solution, and torque ripple elimination by angle shifting of current in other windings also may be obtained. Additionally, it should be noted that the presented fault-tolerant control method can only eliminate the second harmonic torque ripple caused by the main harmonic of current and back EMF voltage, and if the back EMF voltages are non-

sinusoidal, even higher-order harmonic components (up to the 14th order in this article) will be present in the torque in faulty conditions. However, through simulation and experimental results, for non-sinusoidal back-EMF voltages in faulty condition, it has been found that using harmonic current injection strategy along with FTC method has superior results rather than using FOC strategy and injecting the sinusoidal currents. In this study the harmonic content percentage of back-EMF voltage used in HCI strategy is considered to be constant. More exact results may be obtained, if the back-EMF voltage is estimated online.

## REFERENCES

[1] J. Thongam, M. Tarbouchi, A. Okou, D. Bouchard, R. Beguenane, "Trends in naval ship propulsion drive motor technology," IEEE Electrical Power & Energy Conference, 2013, doi:10.1109/EPEC.2013.6802942.

[2] D. Kanturska, "Features in the selection and operation of AC motors for electric propulsion system in ship," 15th International Conference on Electrical Machines, Drives and Power Systems, 2017, doi: 10.1109/ELMA.2 017.7955438.

[3] D. Benatti, C. Alosa, E. Carfagna, F. Immovilli, E. Lorenzani, "Assessment of master-slave and droop control strategies in multi-three-phase drives," IEEE Workshop on Electrical Machines Design, Control and Diagnosis, 2021, doi: 10.1109/WEMDCD51469.2021 .9425685.

[4] Y. Mingqing, M. Hongwei, R. Jingpan, "Research on control strategy of diode clamped three-level 12-phase permanent magnet synchronous motor," Chinese Automation Congress, 2020, doi: 10.1109/CAC51589.2020.9327262.

[5] H. Park, T. Kim, Y. Suh, "Fault-tolerant control methods for reduced torque ripple of multiphase BLDC motor drive system under open-circuit faults," IEEE Transactions on Industry Applications, vol. 58, no. 6, pp. 7275-7285, 2022, doi: 10.1109/TIA.2022.3191633.

[6] Z. Wangguang, D. Wang, Y. Wang, L. Lie, "A review on fault-tolerant control of PMSM," Chinese Automation Congress, 2017, doi: 10.1109/CAC.2017.8243452.

[7] Y. Jeong, S. Sul, S. Schulz, "Fault detection and fault-tolerant control of interior permanent-magnet motor drive system for electric vehicle," IEEE Transactions on Industry Applications, vol. 41, no. 1, pp. 46-51, 2005, doi: 10.1109/TIA.2004.840947.

[8] R. De, C. Jacobina, D. Cabral, "Fault detection of open-switch damage in voltage-fed PWM motor drive systems," IEEE Transactions on Power Electronics, vol. 18, no. 2, pp. 587-593, 2003, doi: 10.1109/TPEL.2003.809351.

[9] F. Meinguet, X. Kestelyn, E. Semail, J. Gyselinck, "Fault detection, isolation and control reconfiguration of three-phase PMSM drives," IEEE International Symposium on Industrial Electronics, 2011, doi: 10.1109/ISIE.2011.5984483.

[10] F. Barrero, M. Duran, "Recent advances in the design, modeling, and control of multiphase machines—part I," IEEE Trans. on Industrial Electronics, vol. 63, no. 1, pp. 449-458, 2016, doi: 10.1109/TIE.2015.2447733.

[11] S. Kallio, M. Andriollo, A. Tortella, J. Karttunen, "Decoupled d-q model of double-star interior-permanent-magnet synchronous machines," IEEE Transactions on Industrial Electronics, vol. 60, no. 6, pp. 2486-2494, 2013, doi: 10.1109/TIE.2012.2216241.

[12] Y. Hu, Z. Zhu, M. Odavic, "Comparison of two-individual current control and vector space decomposition control for dual three-phase PMSM," IEEE Transactions on Industry Application, vol. 53, no. 5, pp. 4483-4492, 2017, doi: 10.1109/TIA.2017.2703682.

[13] A. Almarhoon, "Sensorless control of dual three-phase permanent magnet synchronous machine drives," Ph.D. Thesis, The University of Sheffield, 2016, doi: 10.3390/en16031326.

[14] L. Rocha, E. Silva, P. Silva, G. Prestes, B. Cordeiro, L. Pessoa, R. Vieira, "Evaluation methodology of current control techniques for torque ripple reduction in non-sinusoidal PMSM," IEEE 8th Southern Power Electronics Conference, 2023, doi: 10.1109/SPEC56436.2023.10407773.

[15] M. Nam, J. Kim, K. Cho, H. Kim, Y. Cho, "Torque ripple reduction of an interior pm synchronous motor by compensating harmonic currents based on flux linkage harmonics," Journal of Power Electronics, vol. 17, no. 5, pp. 1223-1230, 2017, doi: 10.6113/JPE.2017.17.5.1223.

[16] S. Mu, J. Kang, Z. Zhong, Z. Ma, "Improved detecting method for multiple rotating reference frames based harmonic control of PMSMs," Chinese Automation Congress, 2020, doi: 10.1109/CAC51589.2020.9327812.

[17] M. Choudri, R. Doncker, R. Loewenherz, N. Fuengwarodsakul, "Concept for distributed field oriented control of twelve-phase permanent magnet machine," IEEE International Conference on Power, Energy and Innovations, 2022, doi: 10.1109/ICPEI55293 .2022.9986964

[18] J. Zhu, J. Yuan, Z. Nie, J. Xu, X. Zeng, "Research on dual 12-Phase 12-slot winding permanent-magnet propulsion system based on All-SiC power module," IEEE Transactions on Industry Applications, vol. 58, no. 6, pp. 7692-7700, 2022, 10.1109/TIA.2022.3202516.

[19] B. Chen, J. Lv, X. Jiang, Y. Zheng, "Model predictive control of a twelve-phase PMSM with simplified cost function," 22nd International Conference on Electrical Machines and Systems, 2019, 10.1109/ICEMS.2019.8922353.

[20] B. Chen, X. Jiang, J. Lv, J. Chai, X. Zhang, S. Sheng, "A decoupled model predictive control method for twelve-phase permanent magnet synchronous motors," IEEE Applied Power Electronics Conference and Exposition, 2020, 10.1109/APEC39645.2020.9124461.

[21] B. Chen, J. Lv, X. Jiang, "Simplified model predictive control of a twelve-phase permanent magnet synchronous motor," 45th Annual Conference of the IEEE Industrial Electronics Society, 2019, 10.1109/IECON.2019.8927027.

[22] A. Niasar, M. Ahmadi, S. Edjtahed, "Sensorless control of non-sinusoidal permanent magnet brushless motor using selective torque harmonic elimination control method based on full-order sliding mode observer," Advances in Power Electronics Journal, vol. 2016, no. 9358604, pp. 1-13, 2016, doi: 10.1155/2016/9358604.

[23] F. Hans, W. Schumacher, S. Chou, X. Wang, "Design of multi frequency proportional–resonant current controllers for voltage-source converters," IEEE Transactions on Power Electronics, vol. 35, no. 12, pp. 13573-13589, 2020, 10.1109/TPEL.2020.2993163.

[24] Z. Zahedipour, M. ShamsiNejad, A. Niasar, H. Eliasi, "Short circuit fault detection in permanent magnet synchronous motor based-on group model of data handling deep neural network," Jordan Journal of Electrical Engineering, vol. 10, no. 2, pp. 169-184, 2024, doi: 10.5455/jjee.204-1686059302.

[25] M. Hadef, M. Mekideche, A. Djerdir, A. N'diaye, "Turn-to-turn short circuit faults between two phases in permanent magnet synchronous motor drives," Jordan Journal of Electrical Engineering, vol. 3, no. 4, pp. 208-222, 2017.

[26] W. Li, J. Lv, X. Jiang, X. Zhang, S. Sheng, "A fault-tolerant control method of 12-phase PMSM in FESS," IEEE 10th International Symposium on Power Electronics for Distributed Generation Systems, 2019, doi: 10.1109/PEDG.2019.8807479.

[27] J. Lv, G. Tian, X. Jiang, "Fault-tolerant control of twelve-phase pmsm based on motor model reconstruction in FESS," IEEE 4th Conference on Energy Internet and Energy System Integration, 2020, doi: 10.1109/EI250167.2020.9347167.

[28] H. Park, Y. Suh, "Fault-tolerant control strategy for reduced torque ripple of independent twelve-phase BLDC motor drive system under open-circuit faults," IEEE Energy Conversion Congress and Exposition, 2020, doi: 10.1109/ECCE44975.2020.9235949.

[29] H. Ghanayem, M. Alathamneh, R. Nelms, "A comparative study of PMSM torque control using proportional-integral and proportional-resonant controllers," IEEE SoutheastCon, 2022, doi: 10.1109/SoutheastCon48659.2022.9764111.